International Journal of Applied Electromagnetics and Mechanics 35 (2011) 281–305
DOI 10.3233/JAE-2011-1359
IOS Press


# Finite element modelling and robust control of fast trilayer polypyrrole bending actuators

Amir Ali Amiri Moghadam[a,*], Keivan Torabi[b] and Majid Moavenian[a]
[a]*Department of Mechanical Engineering, Ferdowsi University of Mashhad, Mashhad, Iran*
[b]*Department of Mechanical Engineering, University of Kashan, Kashan, Iran*

**Abstract.** Conjugated polymer actuators can be employed to achieve micro scale precision positioning, having a wide range of application including biomimetic robots, and biomedical devices. They can operate with low voltage while producing large displacement, in comparison to robotic joints, they do not have friction or backlash, but on the other hand, they have complicated electro-chemo-mechanical dynamics, which makes accurate and robust control of the actuator difficult. There has been extensive research on modeling the electrochemical dynamics of polypyrrole bending actuators. However the mechanical dynamics modeling of actuator remains to be unexplored. In this paper finite element modeling and robust control of fast trilayer polypyrrole bending actuators is proposed. In the modeling part the infinite-dimensional admittance model of actuator will be replaced with a family of linear uncertain transfer functions based on Golubev Method. Further model development will take into account the proper mechanical dynamics, which is essential, when using fast conducting polymer actuators. The purposed modeling approach will be validated based on the existing experimental data. In the controlling part the robust control QFT will be applied to control the highly uncertain dynamics of the conjugated polymer actuators while the actuator carrying variable tip loadings. Finally the analysis of design shows that QFT controller has consistent and robust tracking performance.

Keywords: Fast conjugated polymer actuators, Polypyrrole, FEM, Uncertainty, QFT, Active vibration control

## 1. Introduction

There is an increasing request for new generation of actuators which can be used in devices such as artificial organs, micro robots, human-like robots, and medical applications. Up to now lots of research has been done on developing new actuators such as shape memory alloys, piezoelectric actuators, magnetostrictive actuators, contractile polymer actuators, and electrostatic actuators [1,2]. However conjugated polymer actuators seem to be among the best possible candidates for application in micromanipulation systems since they produce reasonable strain under low input voltage.

The main process which is responsible for volumetric change and the resulted actuation ability of the conjugated polymer actuators is Reduction/Oxidation (RedOx). Thus based on different fabrication form, different configuration of the actuators can be obtained namely: linear extenders, bilayer benders, and trilayer benders [3–5]. By applying a voltage to the actuator, the polypyrrole (PPy) layer on the anode side is oxidized while that on the cathode side is reduced. Ions can transfer inside the Conjugated Polymer Actuators based on two main mechanisms namely diffusion and drift [6]. There are many reports in the literature about potential application of electroactive polymer (EPA) in different robotic systems. Zheng Chen et al. reported the modeling of a robotic fish propelled by an ionic polymer-metal

*Corresponding author. Tel.: +98 9155163197; E-mail: am_am302@stu-mail.um.ac.ir.

composite (IPMC) actuator [7]. Edwin W. H. Jager et al. reviewed the current status of micro actuators based on EPA. They described micro fabrication of these actuators plus the possible application of them in micro systems [8]. We have detailed the dynamic modeling and control of a soft micro robot based on conjugated polymer actuators which could be used in micro manipulation systems [9].

Trilayer polypyrrole actuator, which could operate both in air and liquid environment are promising material for application in micromanipulation systems [10,11]. But before they could be utilize in practical applications, it is essential to understand their dynamics. Especially in applying fast trilayer polypyrrole actuator, we must take into account the proper mechanical dynamics. The main contributions for modeling the mechanical dynamics of the fast trilayer polypyrrole actuator, is mainly limited to presenting and evaluating the experimental data [10–12]. To the best of our knowledge an analytical dynamic model for fast trilayer polypyrrole actuator does not yet exist. In this paper for the first time we will develop a complete dynamic model between the input voltage and output displacement of the fast trilayer polypyrrole actuator. Our complete electro-chemo-mechanical dynamic model consists of a simple third order electro-chemical model which has been achieved based on Golubev Method and a proper electro-mechanical model which has been developed based on the finite element method. Our proposed modeling approaches will be validated based on the existing experimental data [11]. This model can be used both to optimize the open loop displacement of the actuator and to design proper controller, which will lead to practical use of actuator in micro/nano systems.

Application of PID controller for a polypyrrole actuator based on a first order model is presented in [13]. PID and adaptive control approaches based on a first order empirical model are reported in [14]. In our previous works, we have used several approaches for controlling of a polypyrrole actuators [15–17]. In the present work Robust Control QFT will be used for the control of the PPy actuator. The main objective of the controlling section of this paper is to synthesize suitable controller and pre-filter such that, first the closed loop system is stable, second it can track desired inputs, and third it can reject the disturbances. As mentioned before the uncertainty in the dynamics of PPy actuators is inevitable, therefore application of robust control techniques is essential for achieving high precision. There are two basic methodologies for dealing with the effect of uncertainty in a system namely adaptive control and robust control. In adaptive control design approach, the controller will estimate the system's parameter online and then will tune itself based on these estimates. In the robust control design approach, the controller has a fixed structure which will satisfy the system specifications over whole range of plant uncertainty. Although adaptive control can be applied to a wider class of problems, the application of robust control will lead to a simpler controller as the structure of controller is fixed requiring no time for tuning [18].

Thus, the reminder of the paper will be formed as follows:

1) First the classical admittance model of the actuator will be reviewed, and suitable admittance model will be obtained based on Golubev method.
2) The proper mechanical dynamics of the actuator will be obtained based on the finite element method.
3) Finally Robust controller QFT will be designed for tracking problem.

## 2. Trilayer PPy actuator

In this paper as an example of the Conjugated polymer actuators the trilayer PPy actuator will be considered. Figure 1 depicts the trilayer PPy actuator. As the name indicates the trilayer PPy actuator

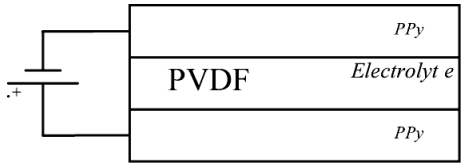


Fig. 1. Three-layer PPy actuator.

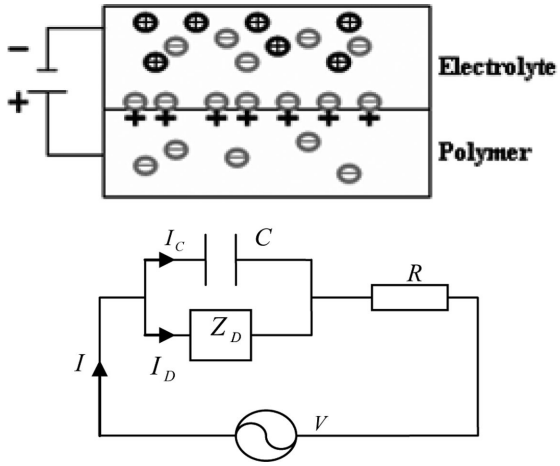


Fig. 2. Description of diffusion and double layer charging and its equivalent electrical circuit.

consists of three layers. The middle layer is Porous Polyvinylidene Fluoride (PVDF) which is used as a storage tank for the electrolyte. And on the both sides of it there are polymer layers (PPy) [19,20].

As it has mentioned before the main process which is responsible for volumetric change of the conjugated polymer actuators is RedOx. Thus in the trilayer bender while the PPy layer on the anode side is oxidized and expands as a result, the PPy layer on the cathode side is reduced and contracts as a result. Therefore this difference in the volume will leads to the bending of the actuator.

## 3. Electro-chemo-mechanical modeling

The electro-chemo-mechanical model is comprised of two parts, namely electrochemical model and electromechanical model.

### *3.1. Electrochemical Modeling*

The electrochemical model relates the input voltage and chemical RedOx reaction inside the PPy actuators. In this part firstly the admittance model for a bilayer actuator will be achieved, and next this model will be extended to the trilayer PPy actuator. Figure 2 depicts the electrical admittance model. Based on the Diffusive-Elastic-Metal model, transportation of ionswithin the polymer is only caused by diffusion [6]. In this part we will briefly review the basic equations of DEM and then propose an uncertain third order model for admittance of the actuator.

According to Fig. 2 and the Kirchhoff's voltage law one has:

$$I(s) = I_c(s) + I_D(s) \tag{1}$$

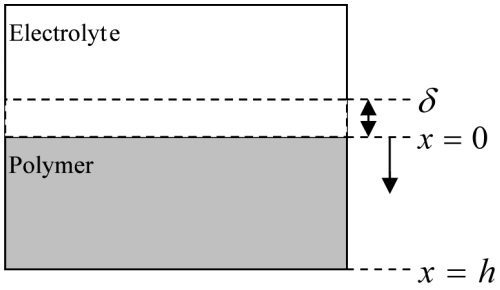


Fig. 3. Description of frame assignment for diffusion.

$$V(s) = I(s).R + \frac{1}{s.C} I_C(s) \tag{2}$$

Where $Z_D$ is the diffusion impedance, $C$ denotes the double-layer capacitance, and $R$ is the electrolyte and contact resistance. Next based on Fig. 3 and the Fick's law of diffusion, diffusion current is:

$$i_D(t) = -F.A.D.\ \left.\frac{\partial c(x,t)}{\partial x}\right|_{x=0} \tag{3}$$

Where $A$ is the surface area of the polymer, $F$ is the Faraday constant, $D$ is the diffusion coefficient, $h$ is the thickness of the PPy layer, and $c$ is the concentration ions. The current of double-layer capacitance is

$$i_C(t) = F.A.\delta.\ \left.\frac{\partial c(x,t)}{\partial t}\right|_{x=0} \tag{4}$$

Where $\delta$ is the double-layer capacitance thickness. And the diffusion equation is

$$\frac{\partial c}{\partial t} = D\frac{\partial^2 c}{\partial x^2} \qquad 0 < x < h \tag{5}$$

Finally the boundary condition is

$$\left.\frac{\partial c(x,t)}{\partial x}\right|_{x=h} = 0 \tag{6}$$

Now based on Eqs (1), (2), (3), (4), (5), and (6), it can be shown that the admittance model ($Y(s) = \frac{I(s)}{V(s)}$) of a conjugated polymer is [6,13].

$$Y(s) = \frac{s\left[\frac{\sqrt{D}}{\delta}\tanh(h\sqrt{s/D}) + \sqrt{s}\right]}{\frac{\sqrt{s}}{C} + Rs^{3/2} + R\frac{\sqrt{D}}{\delta}s\tanh(h\sqrt{s/D})} \tag{7}$$

According to Fig. 1 in the case of a trilayer bender the input voltage is applied across two double-layers, thus the admittance is half of Eq. (7) [22].

$$Y(s)_{tri} = \frac{1}{2}.\frac{s\left[\frac{\sqrt{D}}{\delta}\tanh(h\sqrt{s/D}) + \sqrt{s}\right]}{\frac{\sqrt{s}}{C} + Rs^{3/2} + R\frac{\sqrt{D}}{\delta}s\tanh(h\sqrt{s/D})} \tag{8}$$

Table 1
Values of physical parameters

| Parameter | Value |
|---|---|
| $D$ | $2 \times 10^{-10}$m$^2$/s |
| $h$ | 24 $\mu$m |
| $R$ | 14 $\Omega$ |
| $\delta$ | 27 nm |
| $C$ | $5.23 \times 10^{-5}$ F |

Table 2
The actuator' system poles and zeros based on number of terms used

| No. of Terms | Pole | Zero |
|---|---|---|
| Two | $-0.3793$, $-3.848$, $-2316$ | 0, $-2.736$, $-1069$ |
| Three | $-0.3787$, $-3.741$, $-11.47$, $-2854$ | 0, $-2.524$, $-10.25$, $-1606$, |
| Four | $-0.378$, $-3.696$, $-11.19$, $-23.5$, $-3391$ | 0, $-2.432$, $-9.778$, $-22.29$, $-2145$ |

Because the term tanh, in Eq. (8) is not suitable for real time control of the actuator, in this part the Golubev Method [21] will be used to build a suitable model for control of the actuator. By replacing the term tanh with its equivalent series in Eq. (8) the admittance model is [6]:

$$\frac{I(s)}{V(s)} = \frac{1}{2} \cdot \frac{s}{sR + \dfrac{1}{C(1+\frac{2D}{h\,\delta}\sum\limits_{n=0}^{\infty}\frac{1}{s+\pi^2(2n+1)^2D(2h)^{-2}})}} \tag{9}$$

In the first step one can study Eq. (9) based on its summation term. For this purpose we use the typical values for physical parameters in Table 1.

Based on Table 1, using different values for n (Number of terms in Eq. (9)) Table 2 is acquired.

Accordingly using two terms of Eq. (9), will lead to a third order system. One zero and one pole of this system are located far to the left of the imaginary axis comparing to the other poles and zeros, thus the system can be reduced to a second order system. Similarly using three and four terms will lead to third and fourth order systems respectively. Therefore order of the system depends on the number of terms which are used. In order to solve this problem, the infinite-dimensional system (using tanh) is replaced with a family of uncertain linear systems. Figure 4 compares the admittance of infinite-dimensional model with its estimation based on two, three, and four terms.

For example the parametric model for using three terms is as below:

$$\frac{y(s)}{V(s)} = \frac{a_1 s^4 + a_2 s^3 + a_1 s^2 + a_4 s}{s^4 + b_1 s^3 + b_2 s^2 + b_3 s + b_4} \tag{10}$$

Where

$$Num(s) = \frac{s^4}{2R} + \left(\frac{3}{\delta}\frac{D}{R\,h} + \frac{35}{8}\frac{\pi^2 D}{R\,h^2}\right) s^3 + \left(\frac{35}{2\delta}\frac{\pi^2 D^2}{R\,h^3} + \frac{259}{32}\frac{\pi^4 D^2}{R\,h^4}\right) s^2 + \left(\frac{259}{16}\frac{\pi^4 D^3}{R\,\delta\,h^5} + \frac{225}{128}\frac{\pi^6 D^3}{R\,h^6}\right) s$$

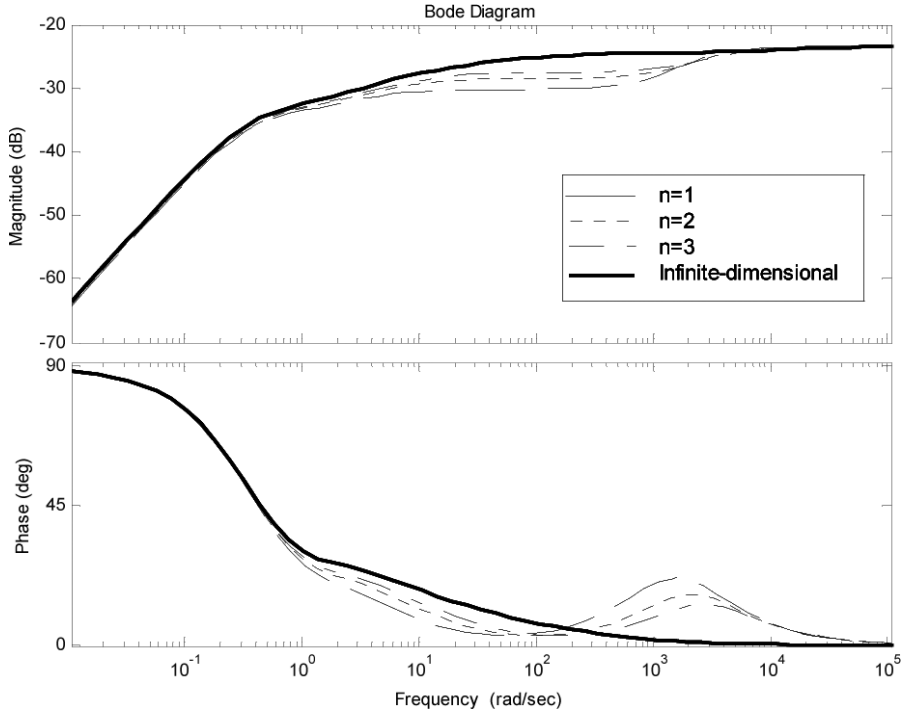


Fig. 4. Comparisons between using different number of terms and the infinite-dimensional model.

$$Den(s) = s^4 + \left(\frac{35}{4}\frac{\pi^2 D}{h^2} + \frac{6 D}{\delta h} + \frac{1}{RC}\right) s^3 + \left(\frac{35}{4}\frac{\pi^2 D}{RC h^2} + \frac{35\pi^2 D^2}{\delta h^3} + \frac{259}{16}\frac{\pi^4 D^2}{h^4}\right) s^2 + \left(\frac{259}{16}\frac{\pi^4 D^2}{RC h^4} + \frac{259}{8}\frac{\pi^4 D^3}{\delta h^5} + \frac{225}{64}\frac{\pi^6 D^3}{h^6}\right) s + \frac{225}{64}\frac{\pi^6 D^3}{RC h^6}$$

Application of the Golubev method involves identifying infinite-dimensional admittance model of the actuator based on different input signals (sin wave, step ...), thus the uncertain admittance transfer function is [17]:

$$\frac{a_1 s^3 + a_2 s^2 + a_3 s}{s^3 + b_1 s^2 + b_2 s + b_3} \tag{11}$$

Where

$a_1 \in [0.05068, 0.06675]; a_2 \in [1.1, 1.211] a_3 \in [2.3, 3.004];$

$b_1 \in [25.63, 26]; b_2 \in [95, 105]; \quad b_3 \in [35, 45]$

It must be noted that the model reduction process used by Yang Fang et al. [22] was based on low frequency application and ignoring high-frequency dynamics, which was useful for predicting the behaviour of ordinary PPy actuators. Since this procedure is not satisfying the dynamics of fast PPy actuators in the whole operating frequency range, in this work an uncertain third order model was chosen to overcome this problem. Figure 5 depicts the admittance Bode plot of Eq. (11). According to Fig. 5 a family of

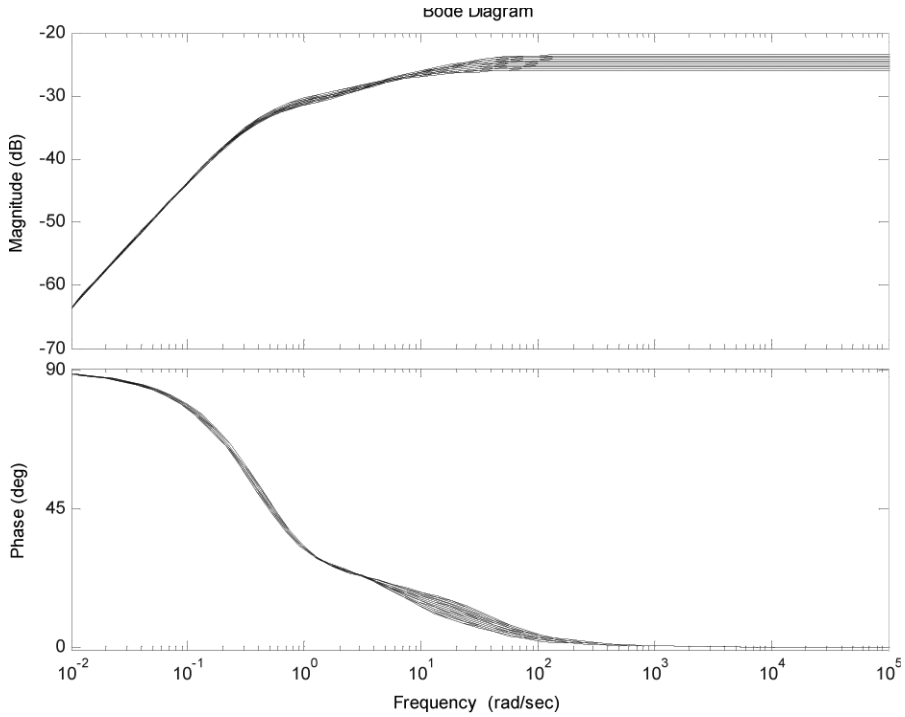


Fig. 5. Admittance Bode plot based on Golubev method.

third order LTI system can predict the admittance model of the actuator in the whole operating frequency range.

### *3.2. Electromechanical modeling*

The electromechanical model relates the input voltage and bending displacement of the PPy actuators. It was experimentally shown that the relation between the induced in-plane strain ($\varepsilon$) and the density of the transferred charges ($\rho$) is as below [23]:

$$\varepsilon = \alpha.\rho \tag{12}$$

Where $\alpha$ is the strain-to-charge ratio. Thus, the induced stress is

$$\sigma = \alpha \,.\, E_{PPy} \,.\, \rho \tag{13}$$

Where $E_{PPy}$ is the Young's modulus of PPy, and $\rho$ can be achieved in the Laplace domain as below [6, 13]:

$$\rho(s) = \frac{I(s)}{s\,W\,L\,h_{PPy}} \tag{14}$$

Where W is the width of the PPy, $h_{PPy}$ is the thickness of the PPy, and L is the length of the PPy. Three layer polymer actuators can bend based on the expansion of the top layer and contraction of the bottom layer. The induced stresses in expanded or contracted layers, are assumed to be the same and in

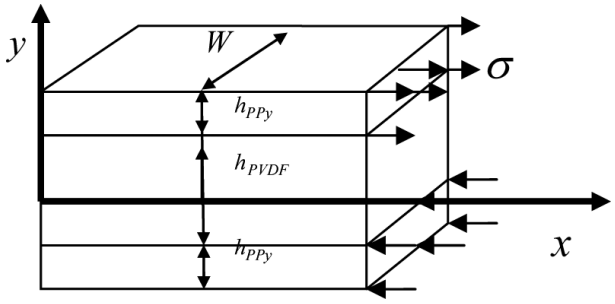


Fig. 6. Distribution of induced stress across the thickness of the trilayer polymer actuator.

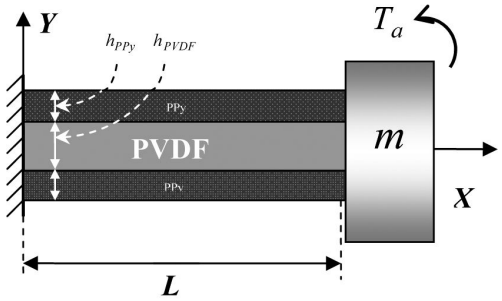


Fig. 7. Consideration of the actuation process an external moment.

the opposite directions. Distribution of the induced stress is approximately constant along the thickness. Additionally application of gold layers on both sides of the PVDF layer diminishes the potential drop along the length of the actuator, thus the actuation process is analogous with the pure bending within the actuator. Based on Fig. 6; one can obtain the bending moment as follow:

$$\begin{aligned} T_a &= 2\int \sigma\, y\, dA \\ &= 2\int E_{PPy}\,\alpha\rho(t)\, y\, dA = 2E_{PPy}\alpha\rho(t)\int y\, dA \\ &= E_{PPy}\alpha\ W\, h_{PPy}(h_{PPy}+h_{PVDF})\,\rho(t) \end{aligned} \tag{15}$$

Therefore the induced actuation process can be modeled with an external moment $T_a$ which applied at the free end of the actuator Fig. 7.

Thus the relation between the input voltage $V$ and the output bending moment $T_a$ is obtained as below:

$$\frac{T_a(s)}{V(s)} = \frac{1}{2L}\cdot\frac{E_{PPy}\alpha\ \ (h_{PPy}+h_{PVDF})}{sR+\frac{1}{C(1+\frac{\sqrt{D}}{\delta\sqrt{s}}\tanh(h\sqrt{\frac{s}{D}}))}} \tag{16}$$

### *3.3. Finite element modeling*

In the next step a proper mechanical dynamics model between the input moment and output displacement will be derived based on finite element method.

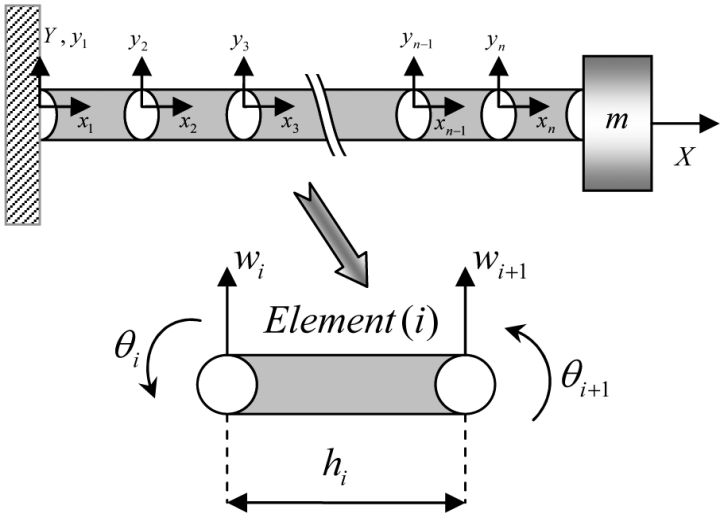


Fig. 8. Schematic of fast PPy actuator with $n$ elements.

According to Fig. 8 the PPy actuator can be considered to have $n$ elements. The lateral displacement in the element $i$ can be defined as below [24,25]:

$$y_i(x,t) = \{N(x)\}^T \{u(t)\}_i \tag{17}$$

Where $\{N\}$ is a $4 \times 1$ vector of Hermite polynomials, and$\{u(t)\}_i = [w_i,\ h_i\theta_i,\ w_{i+1},\ h_i\theta_{i+1}]^T$. It must be noted that the local frame in each element has the same orientation as the global frame, thus the vector of nodal displacement in local and global fames is the same ($\{\overline{u}(t)\}_i = \{u(t)\}_i$). Based on the above definitions we can derive the kinetic energy of the element $i$ as follow:

$$\begin{aligned} T_i(t) &= \frac{1}{2}\int_0^{h_i} \left[(\rho A)_{PVDF} + 2(\rho A)_{PPy}\right] \left[\frac{\partial y_i(x,t)}{\partial t}\right]^2 dx \\ &= \frac{1}{2}\int_0^{h_i} \left[(\rho A)_{PVDF} + 2(\rho A)_{PPy}\right] \left[\{\dot{u}(t)\}_i^T \{N(x)\} \{N(x)\}^T \{\dot{u}(t)\}_i\right] dx \\ &= \frac{1}{2} \{\dot{u}(t)\}_i^T [M]_i \{\dot{u}(t)\}_i \end{aligned} \tag{18}$$

Where

$$[M]_i = \int_0^{h_i} \left[(\rho A)_{PVDF} + 2(\rho A)_{PPy}\right] \left[\{N(x)\} \{N(x)\}^T\right] dx \tag{19}$$

Additionally $(\rho A)_{PVDF}$, and $(\rho A)_{PPy}$ are the products of density by the cross-sectional area of PVDF and PPy layers respectively. It must be noted that if we attach a load ($m$) to the tip of the actuator we must modify the kinetic energy of the last element by adding the term $\frac{1}{2} m \left[\frac{\partial y_n(x,t)}{\partial t}|_{x=h_n}\right]^2$. Thus the mass matrix of the last element is

$$\begin{aligned} [M]_n = &\int_0^{h_n} \left[(\rho A)_{PVDF} + 2(\rho A)_{PPy}\right] \left[\{N(x)\} \{N(x)\}^T\right] dx \\ &+ m \{N(h_n)\} \{N(h_n)\}^T \end{aligned} \tag{20}$$

Similarly the potential energy of the element $i$ can be defined as below:

$$\begin{aligned} V_i(t) &= \frac{1}{2}\int_0^{h_i} \left[(EI)_{PVDF} + 2(EI)_{PPy}\right] \left[\frac{\partial^2 y_i(x,t)}{\partial x^2}\right]^2 dx \\ &= \frac{1}{2}\int_0^{h_i} \left[(EI)_{PVDF} + 2(EI)_{PPy}\right] \left[\{u(t)\}_i^T \left\{N''(x)\right\} \left\{N''(x)\right\}^T \{u(t)\}_i\right] dx \\ &= \frac{1}{2}\{u(t)\}_i^T [K]_i \{u(t)\}_i \end{aligned} \tag{21}$$

Where

$$[K]_i = \frac{1}{2}\int_0^{h_i} \left[(EI)_{PVDF} + 2(EI)_{PPy}\right] \left[\left\{N''(x)\right\} \left\{N''(x)\right\}^T\right] dx \tag{22}$$

Additionally $(EI)_{PVDF}$, and $(EI)_{PPy}$ are the flexural rigidity of the PVDF and PPy layers respectively. The vector of nodal forces can be obtained based on the principal of the virtual work:

$$\begin{aligned} \delta \overline{W}_i(t) &= \int_0^{h_i} T_a(t)\, \delta \left[\frac{\partial y_i(x,t)}{\partial x}\right] dx = \int_0^{h_i} T_a(t) \left\{N'(x)\right\}^T \delta \{u(t)\}_i dx \\ &= T_a(t) \{f\}_i^T \delta \{u(t)\}_i \end{aligned} \tag{23}$$

Where

$$\{f\}_i = \int_0^{h_i} \left\{N'(x)\right\} dx \tag{24}$$

Achieving the mass and stiffness matrices for the elements we must assemble them to analyze the actuator. By using $n$ elements the vector of nodal displacement for the complete system ($\left\{\overline{U}\right\}$) has $2(n+1)$ degrees of freedom. In order to assemble the elements the extended vector of the nodal displacement for an element $i$ can be defined as follow:

$$\left\{\overline{U}(t)\right\}_i = [0_{1\times 2(i-1)}\,,\, \{u(t)\}_i^T\,,\, 0_{1\times 2(n-i)}]^T \tag{25}$$

Similarly the extended vector of nodal forces ($M(t)\left\{\overline{F}\right\}_i$) and extended matrices of mass and stiffness ($\left[\overline{M}\right]_i$, $\left[\overline{K}\right]_i$) can be achieved [25]. Next based on the Lagrange's equations the discrete set of equations which describe the dynamic of the actuator is derived as follows:

$$\left[\overline{M}\right] \left\{\ddot{\overline{U}}\right\} + \left[\overline{K}\right] \left\{\overline{U}\right\} = T_a(t) \left\{\overline{F}\right\} \tag{26}$$

Where $\left[\overline{M}\right] = \sum_{i=1}^{n} \left[\overline{M}\right]_i$, $\left[\overline{K}\right] = \sum_{i=1}^{n} \left[\bar{K}\right]_i$, and $\left\{\overline{F}\right\} = \sum_{i=1}^{n} \left\{\overline{F}\right\}_i$. Due to the fixed boundary condition at the first element we must eliminate the first and second rows and columns of the extended mass and stiffness matrices. Thus the reduced form of the motion equations is:

$$\left[\overline{M^*}\right] \left\{\ddot{\overline{U}^*}\right\} + \left[\overline{K^*}\right] \left\{\overline{U}^*\right\} = T_a(t) \left\{\overline{F}^*\right\} \tag{27}$$

Modal analysis will be used to determine the solution of Eq. (27). One can obtain the natural frequencies of the actuator by solving the eigenvalue problem:

$$\left[\overline{K}^*\right]\ \{V\} = \Lambda\ \left[\overline{M}^*\right]\ \{V\}\ ,\qquad \Lambda = \omega^2 \tag{28}$$

Where $\Lambda$ is eigenvalue, and $\{V\}$ is the eigenvector which must be normalized with respect to the mass matrix as below:

$$\{V\}_r^T\ \left[\overline{M}^*\right]\ \{V\}_s = \delta_{rs}\quad r,s = 1,2,\ldots,2n \tag{29}$$

Considering $[V] = [\{V\}_1, \{V\}_2 \cdots\ \{V\}_{2n}]$, it can be easily shown that:

$$[V]^T\ \left[\overline{M}^*\right]\ [V] = [1]\quad [V]^T\ \left[\overline{K}^*\right]\ [V] = \left[\omega^2\right] \tag{30}$$

According to the experimental data [11] the polymer actuator has a low damping ratio (approximately 0.03).

We use proportional damping model here as follow:

$$\left[\overline{C}^*\right] = \alpha\ \left[\overline{M}^*\right] + \beta\ \left[\overline{K}^*\right] \tag{31}$$

Where $\alpha$, and $\beta$ are constant. Let us define C as:

$$[C] = [V]^T\ \left[\overline{C}^*\right]\ [V] = \alpha\,[1] + \beta\,\left[\omega^2\right] = [2\varsigma\omega] \tag{32}$$

Considering the damping effects the Eq. (24) can be rewrite as below:

$$\left[\overline{M}^*\right]\left\{\ddot{\overline{U}}^*\right\} + \left[\overline{C}^*\right]\ \left\{\dot{\overline{U}}^*\right\} + \left[\overline{K}^*\right]\ \left\{\overline{U}^*\right\} = T_a(t)\left\{\overline{F}^*\right\} \tag{33}$$

Now by defining:

$$\left\{\overline{U}^*\right\} = [V]\ \{\eta(t)\} \tag{34}$$

And multiplying both sides of Eq. (33), by $[V]^T$ we have:

$$\ddot{\eta}_i(t) + 2\varsigma\omega_i\dot{\eta}(t) + \omega_i^2\eta_i(t) = Q_i(t) \tag{35}$$

Where

$$\{Q(t)\} = [V]^T\,T_a(t)\left\{\overline{F}^*\right\} \tag{36}$$

By applying the Laplace operator to the Eq. (35) we have:

$$\eta_i(s) = \frac{Q_i(s)}{s^2 + 2\varsigma\omega_i s + \omega_i^2} \tag{37}$$

Considering that $\overline{U}_i^*(s) = \sum\limits_{j=1}^{2n}\eta_j(s)\,V_{ij}$ and, $Q_i(s) = T_a(s)\sum\limits_{j=1}^{2n}V_{ji}\overline{F}_j^* = T_a(s)\overline{Q}_i$ we have:

$$\overline{U}_i^*(s) = T_a(s)\sum_{j=1}^{2n}\frac{\overline{Q}_j}{s^2 + 2\varsigma\omega_j s + \omega_j^2}V_{ij} \tag{38}$$

Table 3
Values of physical parameters

| Parameter | Value |
|---|---|
| $h_{PPy}$ | 24 $\mu$m |
| $h_{PVDF}$ | 110 $\mu$m |
| $E_{PPy}$ | 80 MPa |
| $E_{PVDF}$ | 312 MPa |
| $L$ | 25 mm |
| $W$ | 2 mm |

Table 4
Experimental and obtained resonant frequencies

| Mode | Fundamental (Hz) | 2nd (Hz) | 3rd (Hz) |
|---|---|---|---|
| Experimental | 14.2 | 89.5 | 252.1 |
| One element | 14.2679 | 140.577 | – |
| Two elements | 14.2073 | 89.7476 | 303.5426 |
| Five elements | 14.2006 | 89.0369 | 250.0763 |
| Six elements | 14.2005 | 89.0143 | 249.6372 |
| Seven elements | 14.2004 | 89.0064 | 249.4349 |

Table 5
Fundamental natural frequencies for variation of the tip loadings

| Tip mass (mg) | Fundamental Natural frequency (Hz) |
|---|---|
| 0 | 14.2018 |
| 10 | 6.3753 |
| 30 | 3.9496 |
| 40 | 3.4532 |

Therefore the dynamic model between the input moment and output displacement in the last element is:

$$\frac{y(x,s)}{T_a(s)} = \left\{\overline{U}^*_{2n-3}, \overline{U}^*_{2n-2}, \overline{U}^*_{2n-1}, \overline{U}^*_{2n}\right\}\{N(x)\} \tag{39}$$

Consequently Eqs (16) and (39) will construct a complete model between the input voltage to the actuator and its output displacement. The natural frequencies of the polymer actuator are obtained, based on the physical parameters in Table 3, and Eq. (28).

In order to validate our model we compare the experimental results reported in [11], with the obtained resonant frequencies using Eq. (28). Table 4 shows that our model could predict the resonant frequencies well. According to the table a model with six elements converges which will be used in the simulations. Figure 9 illustrates the mode shapes corresponding to five lowest natural frequencies of the actuator. Figure 10 depicts the bode plot between the input voltage and the output displacement of the actuator.

Figure 11 compares the magnitude bode plot of the experimental results reported in [11] with our theoretical model which indicates that our purposed model can predicts the actuator behavior well.

We have also considered the effects of tip load variation and obtained the fundamental natural frequencies of the actuator for carrying different loads. According to Fig. 12 and Table 5 increase of the tip mass from 0 to 40 mg will decrease the fundamental natural frequency which is consistent with the reported experimental data in [11].

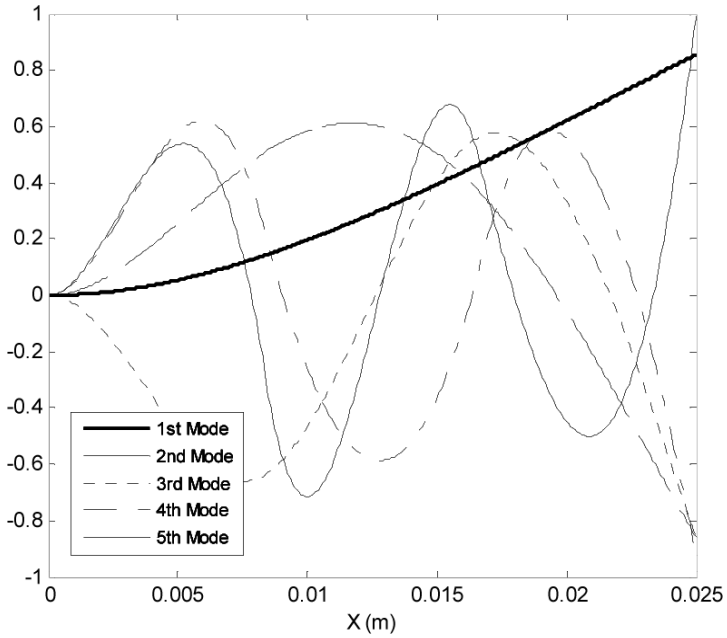


Fig. 9. First five mode shapes of the actuator.

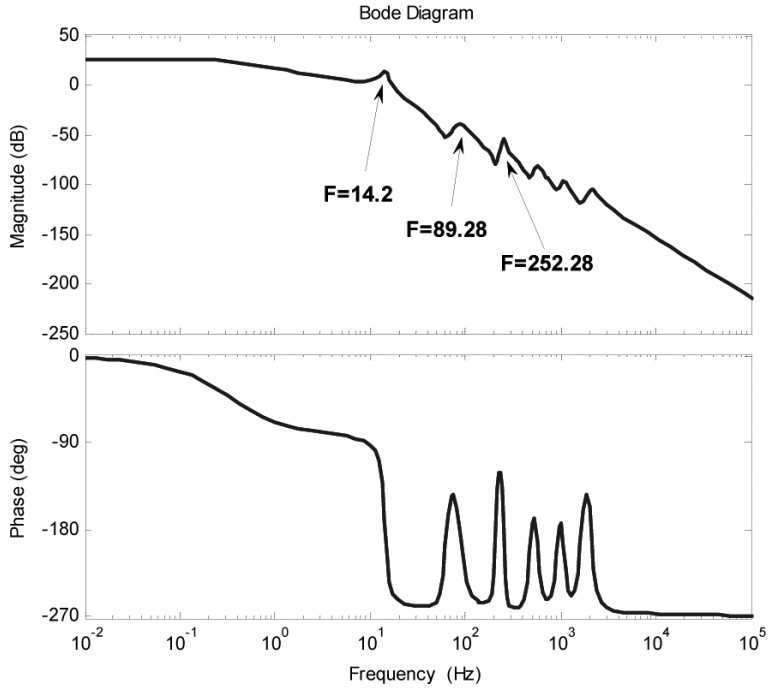


Fig. 10. Bode plot between the input voltage and the output displacement of the actuator.

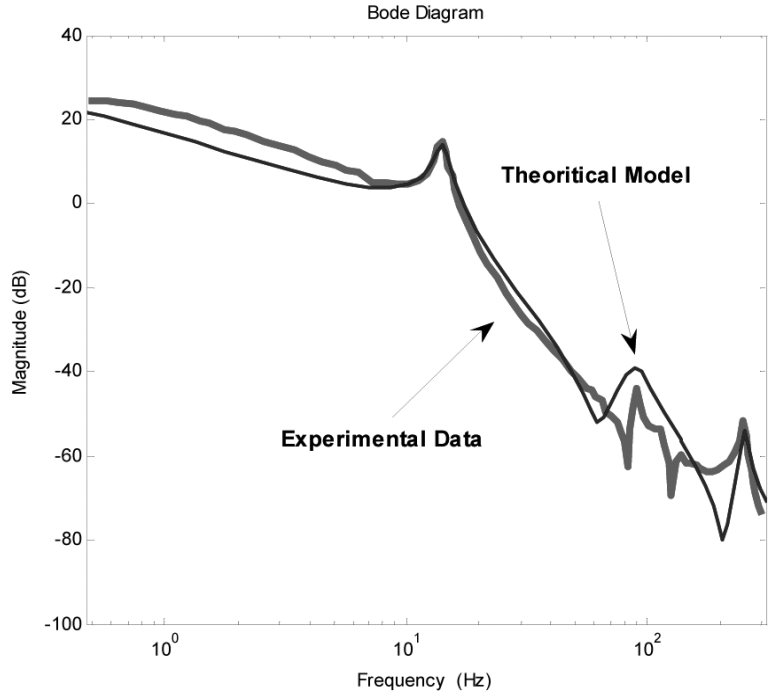


Fig. 11. Bode plot between the input voltage and the output displacement of the actuator.

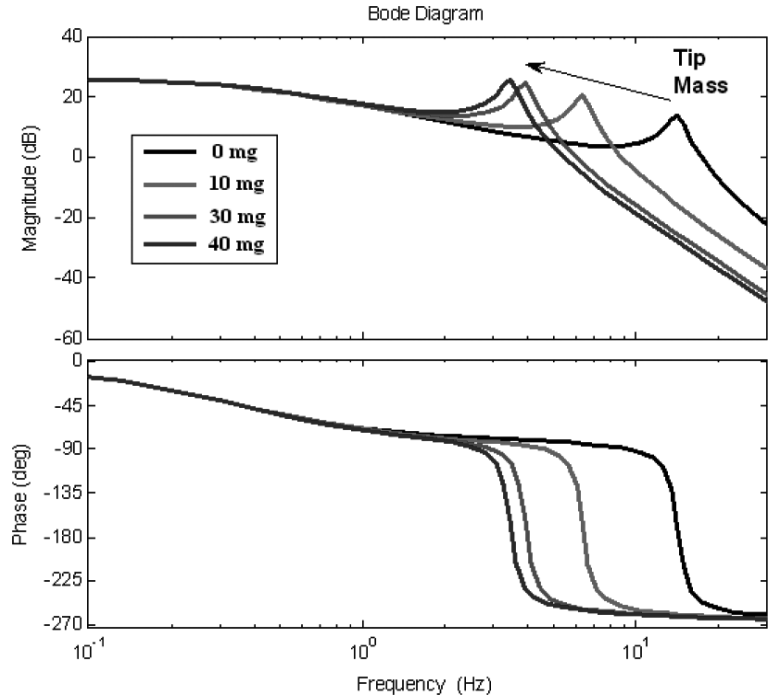


Fig. 12. Bode plot between input voltage and the output displacement of the fast PPy actuator with 0, 10, 30, and 40 mg tip mass. The arrow illustrates tip mass increasing.

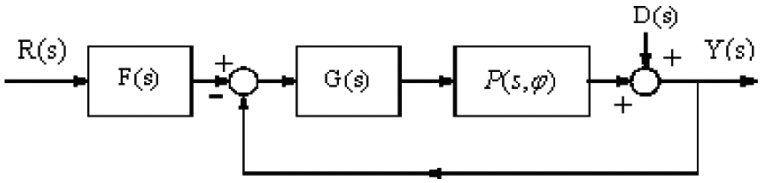


Fig. 13. Two degree of freedom feedback system.

## 4. Application of QFT

There are many practical systems that have high uncertainty in open-loop transfer functions which makes it very difficult to have suitable stability margins and good performance in command following problems for the closed-loop system. Therefore a single fixed controller in such systems is found among "robust controllers" family.

Quantitative Feedback Theory (QFT) is a robust feedback control-system design technique initially introduced by Horowitz (1963, 1979), which allows direct design to closed-loop robust performance and stability specifications. Since then this technique has been developed by him and others [26–30].

In many techniques from "robust control" family such as $H_\infty$, design is based on magnitude of transfer function in frequency domain, but QFT is not only concerned with aforementioned subject, but also able to take into account phase information in the design process. The unique feature of QFT is that the performance specifications are expressed as bounds on frequency-response loop shapes in such a way that satisfaction of these bounds imply a corresponding approximate closed-loop satisfaction of some time-domain response bounds for given classes of inputs and for all uncertainty in a given compact set. Consider the feedback system shown in diagram Fig. 13. This system has the two-degrees of freedom structure (consider controller G(s) and prefilter F(s)). In this diagram P(s) is uncertain plant belongs to a set $P(s) \in \{P(s,\varphi); \varphi \in \Phi\}$ where here $\varphi$ is the vector of uncertain parameters, which takes the values in $\Phi$. G(s) is the fixed structure feedback controller and F(s) is the prefilter, and D(s) is the disturbance at the plant output.

The QFT controller design method is briefly summarized as follows:

In parametric uncertain systems, we must first generate plant templates prior to the QFT design (at a fixed frequency, the plant's frequency response set is called a *template*). Given the plant templates, QFT converts closed loop magnitude specifications into magnitude constraints on a nominal open- loop function (these are called QFT *bounds*). A nominal open loop function is then designed to simultaneously satisfy its constraints as well as to achieve nominal closed loop stability. In a two degree-of-freedom design, a pre-filter will be designed after the loop is closed (i.e., after the controller has been designed) [31, 32]. The objective of this section is to design a robust controller for a fast trilayer polypyrrole bending actuators that carrying a variable tip mass. Especially the tip mass will vary from 0 to 30 mg. The actuator physical parameters are presented in Tables 1, 3. According to Table 5 the worst case belongs to the tip load of 30 mg with the fundamental natural frequency of 3.9496 Hz. Suitable controller and pre-filter are to be designed having the following properties:

First the closed loop system is stable: The robust margin is that the magnitude of closed loop system for all considered uncertainty must be less than 1.1.

Second it can track desired inputs: Robust tracking specification based on suitable performance of actuator is overshoot ($= 5\%$) and the settling time ($= 0.4$s) for all plant uncertainty.

Third it can reject the disturbances: The magnitude of the closed loop system for the input and output disturbances must be less than 0.1.

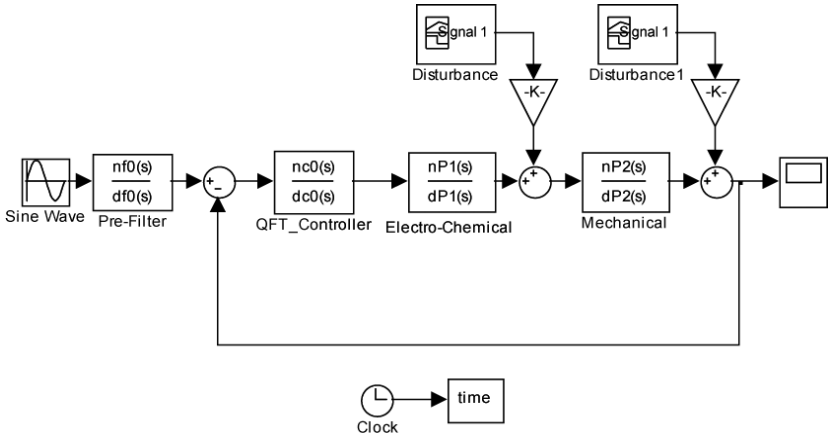


Fig. 14. QFT controlling block diagram.

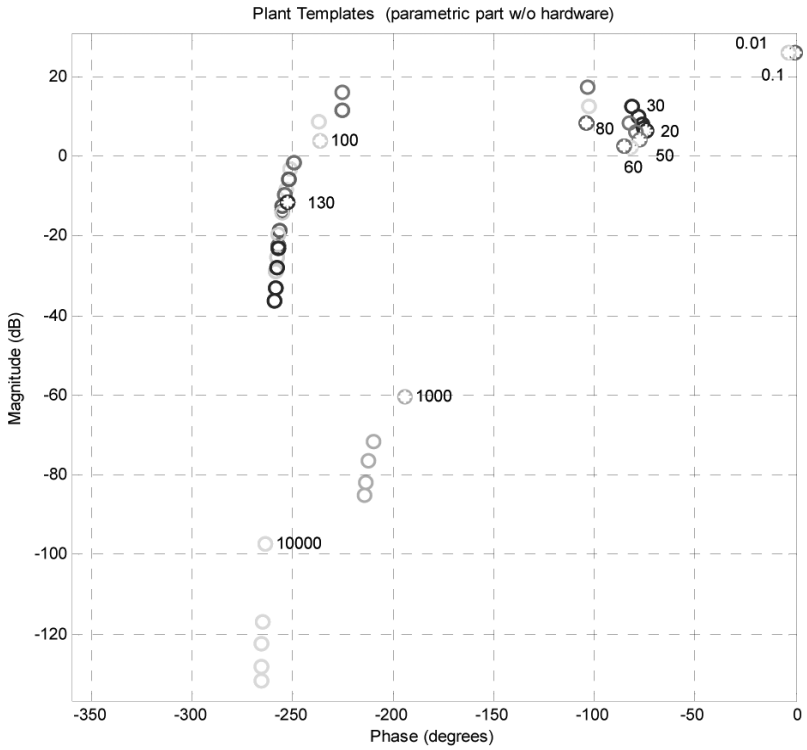


Fig. 15. The boundary of the plant templates.

At the first step we must define the plant uncertainty (template), which is shown in Fig. 15. Then having the robust performance bounds in the loop-shaping phase of design suitable controller and Pre-filter can be achieve as follows:

$$G_1 = \frac{3.24 \times 10^{10} s^3 + 1.49 \times 10^{11} s^2 + 1.95 \times 10^{13} s + 2.5 \times 10^{13}}{s^3 + 2.1 \times 10^{7} s^2 + 1.32 \times 10^{12} s + 7.36 \times 10^{13}} \tag{40}$$

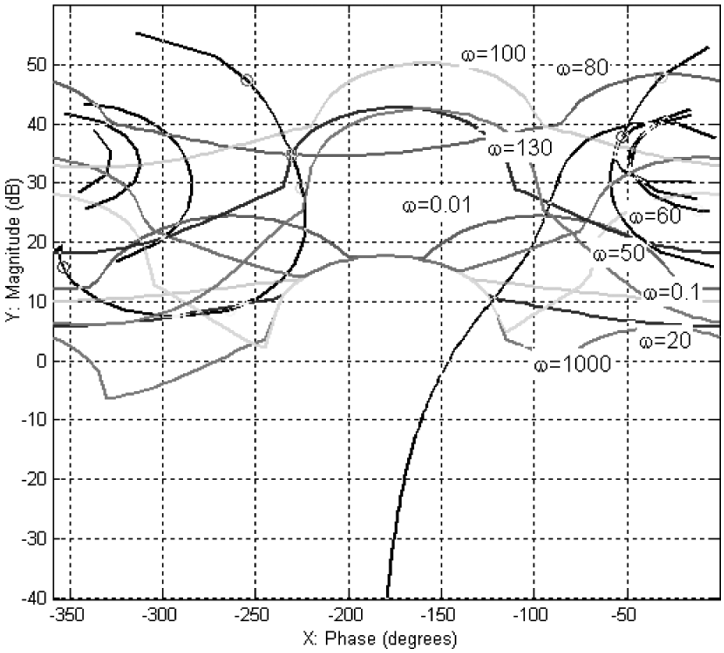


Fig. 16. Loop shaping of open-loop system.

$$F = \frac{120.62}{s^2 + 24.53s + 110.12} \tag{41}$$

Figure 14 illustrates the QFT controlling block diagram

Figure 16 depicts the loop-shaping of open loop system. It can be observed that the nominal plant lies on its performance bounds which confirm the correctness of design.

Figure 17 shows time domain simulation for unit step responses. Figure 18 gives the satisfaction of desired tracking specifications in the frequency domain.

Figure 19 shows a step disturbance at the plant input, while Fig. 20 depicts the response of the uncontrolled and QFT control system to the disturbance. Figure 21 illustrates the control effort for all considered uncertainty under the step disturbance at the plant input.

Figure 22 shows the tracking problem for the reference input$R = \sin(0.5\,\pi\,t) + \sin(2\pi\,t)\ (mm)$, while Fig. 23 depicts the tracking error. Figures 24–25 show the control effort and current output of the actuator for the input $R = \sin(0.5\,\pi\,t) + \sin(2\pi\,t)\ (mm)$.

Figure 26 shows the tracking problem for a square wave input, while Fig. 27 depicts the tracking error. Figures 28–29 show the control effort and current output of the actuator under a square wave input.

## 5. Conclusions

In this paper robust control QFT is applied to control the fast trilayer polypyrrole bending actuator with variable tip loadings. The main contributions in the modeling part are:

Replacing infinite-dimensional admittance model of PPy actuators with a family of Linear Time Invariant systems based on Golubev Method which:

a-facilitates the real time control, b- predicts the admittance dynamic in whole operating frequency range.

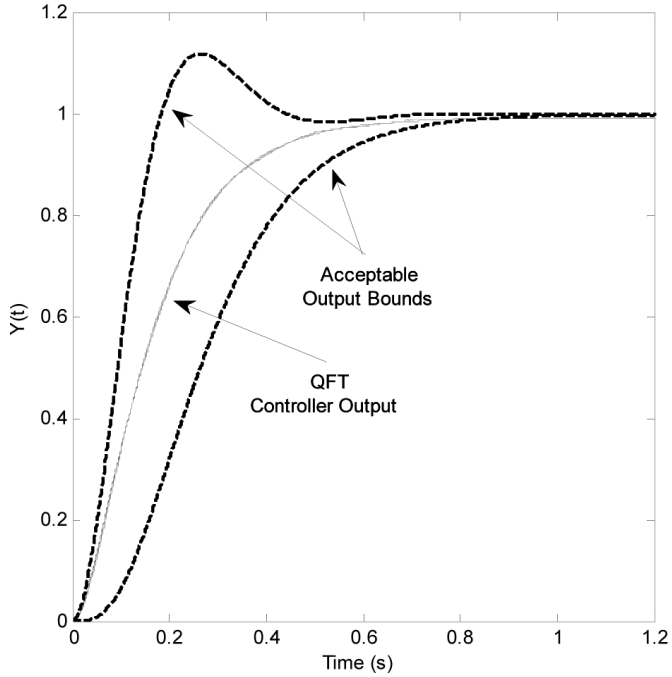


Fig. 17. Unit step response for all considered uncertainty with acceptable output bounds.

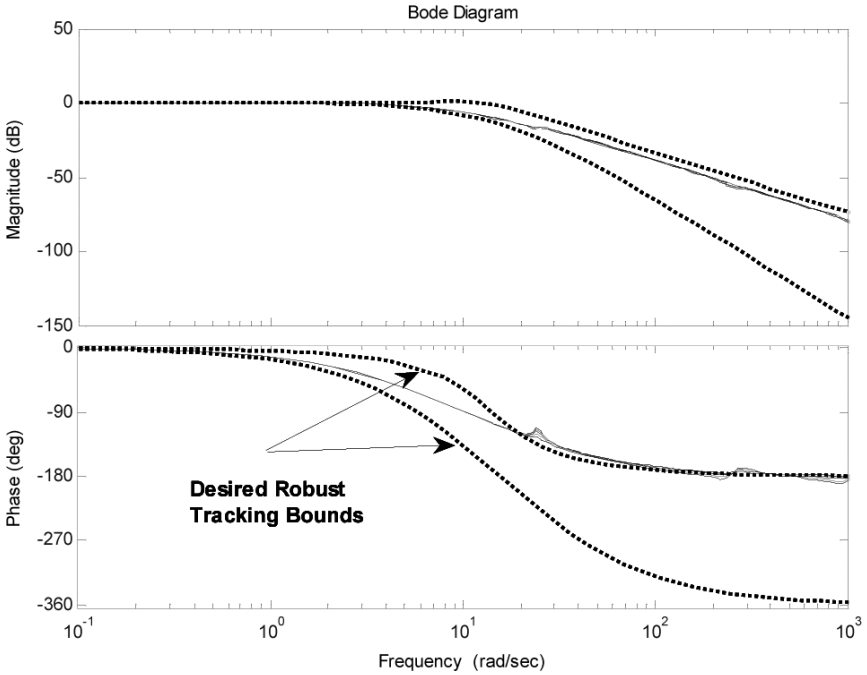


Fig. 18. Closed-loop frequency response with pre-filter.

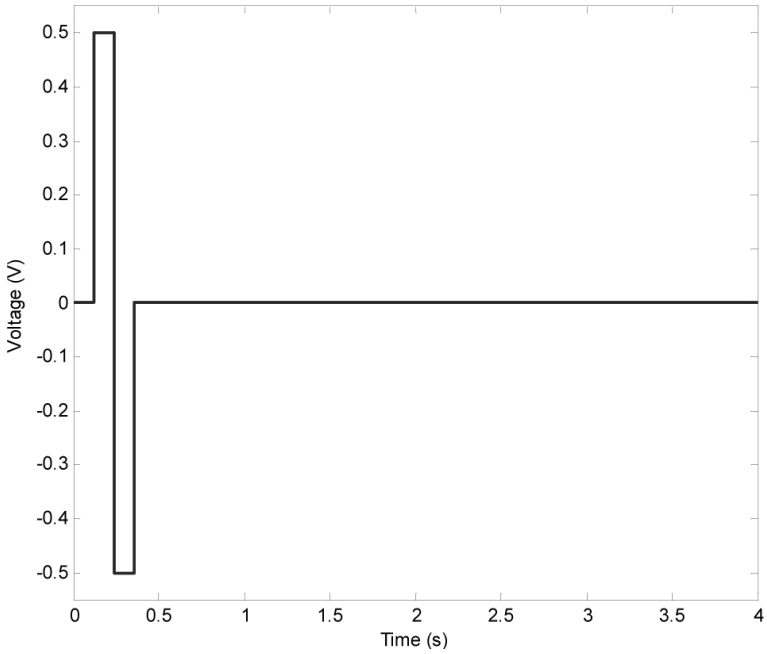


Fig. 19. Step disturbance at the plant input.

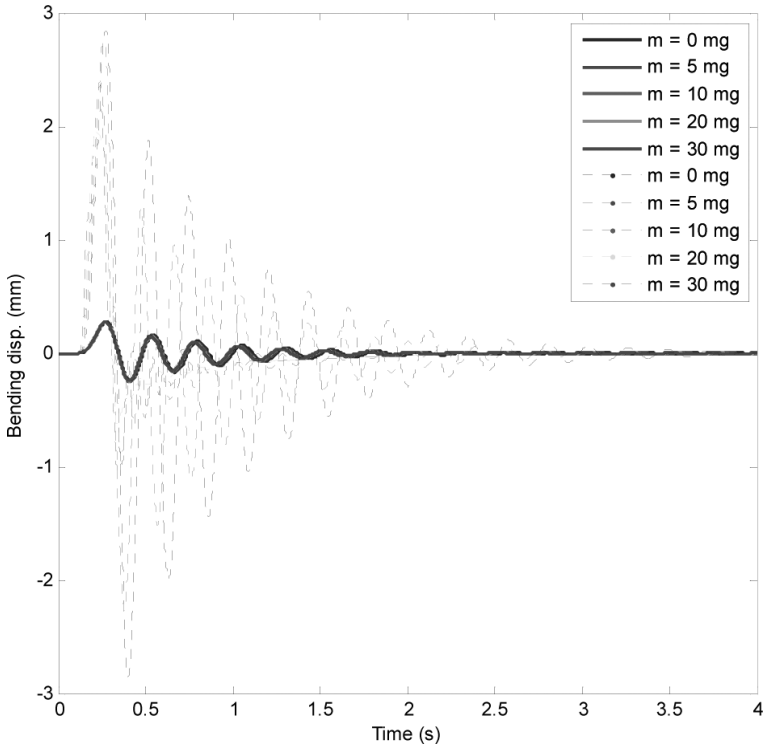


Fig. 20. Uncontrolled (Dashed lines) and QFT controller response (Solid lines) to a step disturbance at the plant input for all considered uncertainty.

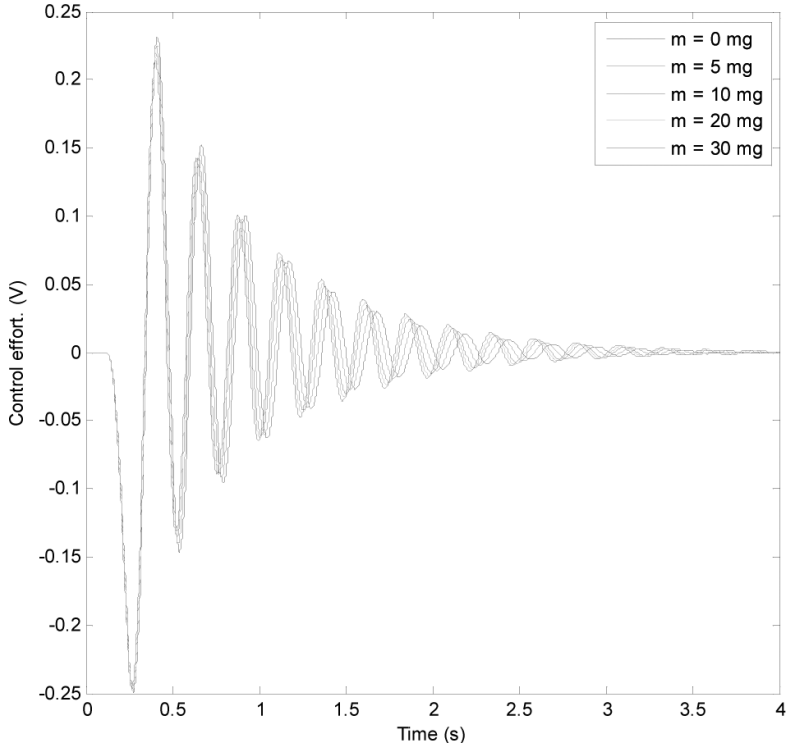


Fig. 21. Control effort for all considered uncertainty under the step disturbance at the plant input.

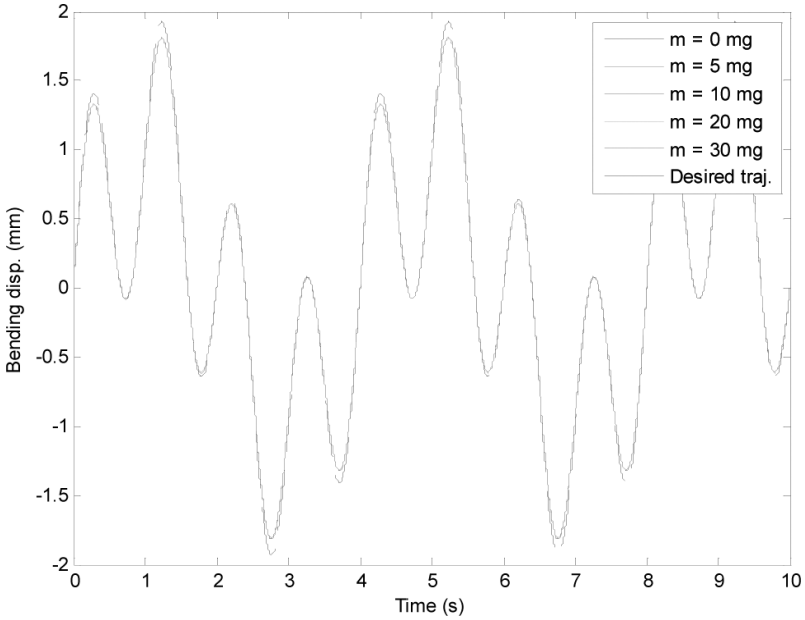


Fig. 22. Tracking problem for a sin wave.

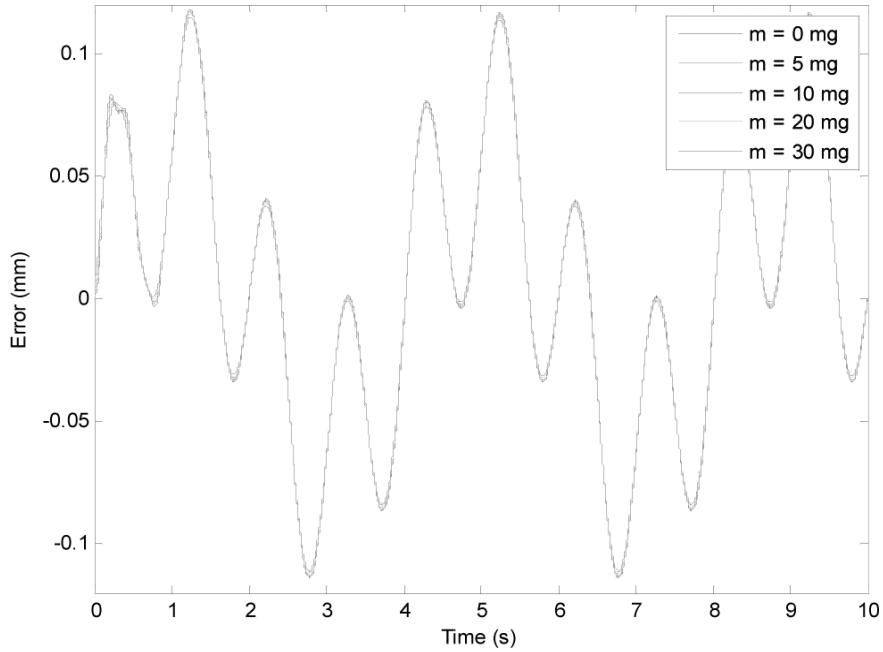


Fig. 23. Tracking error under the reference input$R = \sin(0.5\,\pi\,t) + \sin(2\pi\,t)\ (mm)$.

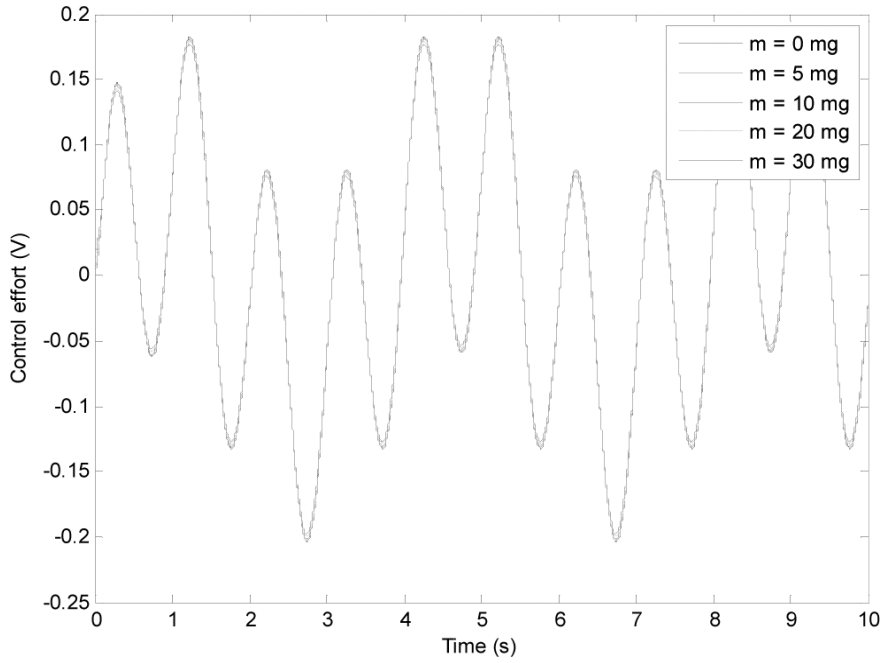


Fig. 24. Control effort for all considered uncertainty under the reference input $R = \sin(0.5\,\pi\,t) + \sin(2\pi\,t)\ (mm)$.

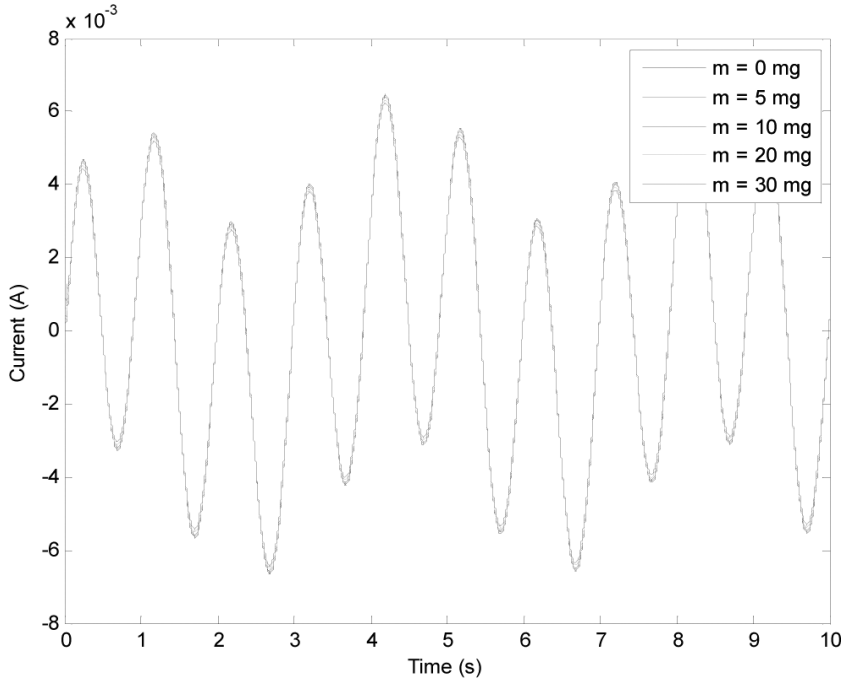


Fig. 25. Current output of the actuator all considered uncertainty under the reference input $R = \sin(0.5\,\pi\,t) + \sin(2\pi\,t)\ (mm)$.

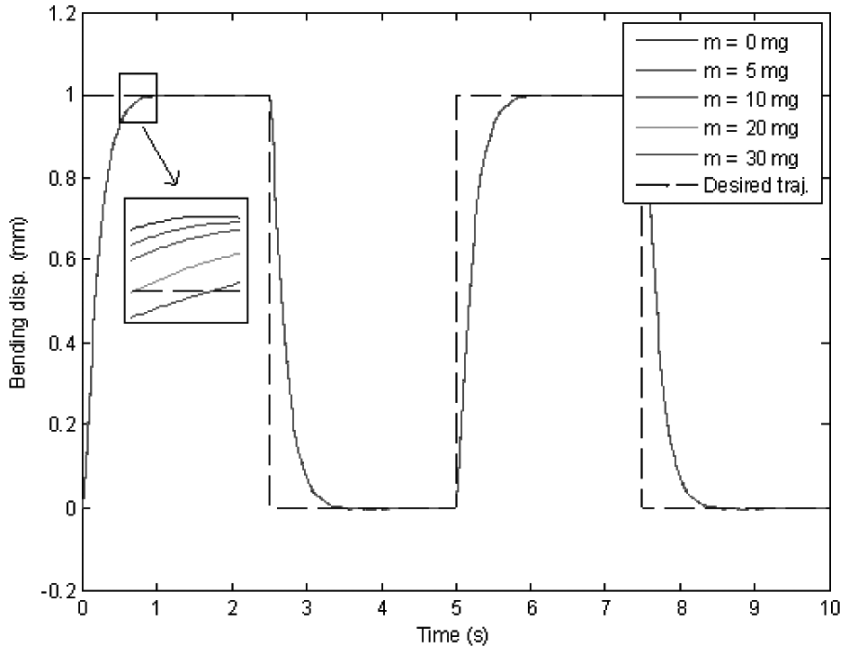


Fig. 26. Tracking problem for a square wave input.

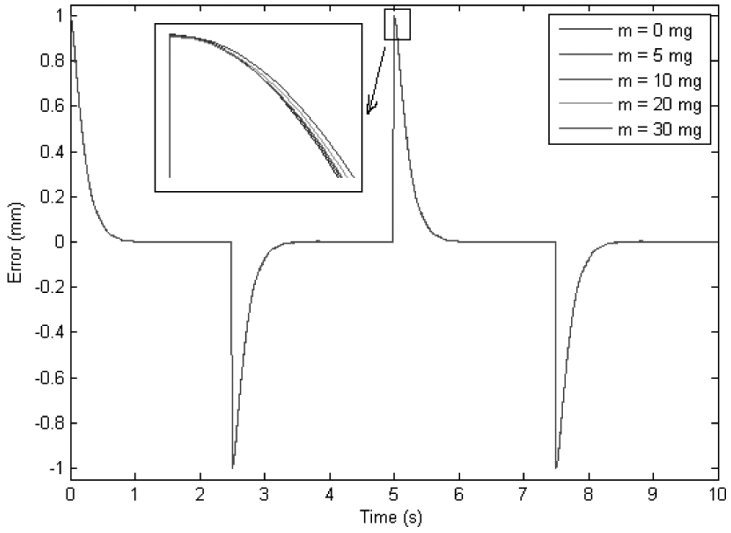


Fig. 27. Tracking error for a square wave input.

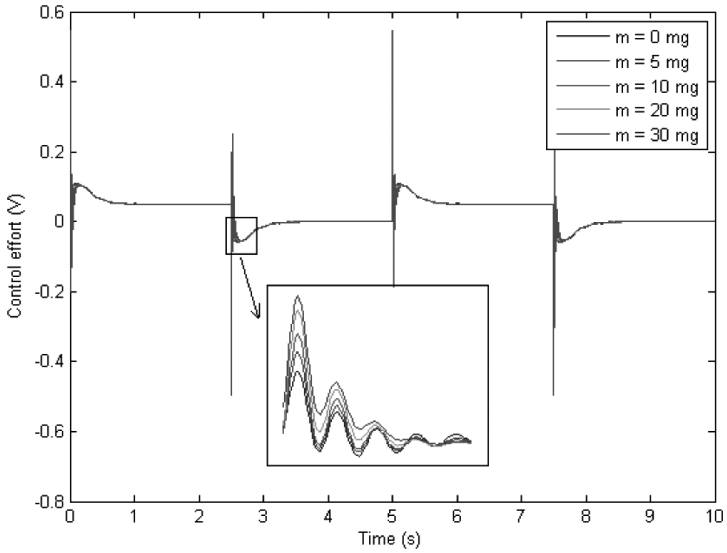


Fig. 28. Control effort for all considered uncertainty under a square wave input.

Proposing a finite element method for modeling the mechanical dynamics of fast trilayer polypyrrole bending actuators, this is consistence with the existing experimental data [11]. Additionally compensates the weaknesses of the previous modeling attempt [20]. Therefore we have developed a complete model between the input voltage and output displacement of the actuator. This model can be used both to optimize the open loop displacement of the actuator and to design proper controller, which will lead to practical use of actuator in micro/nano systems.

In the controlling part it is shown that:

The robust control QFT can successfully be applied to control the highly uncertain dynamics of PPy actuator. Especially we have designed a controller which is robust against the uncertain dynamics of

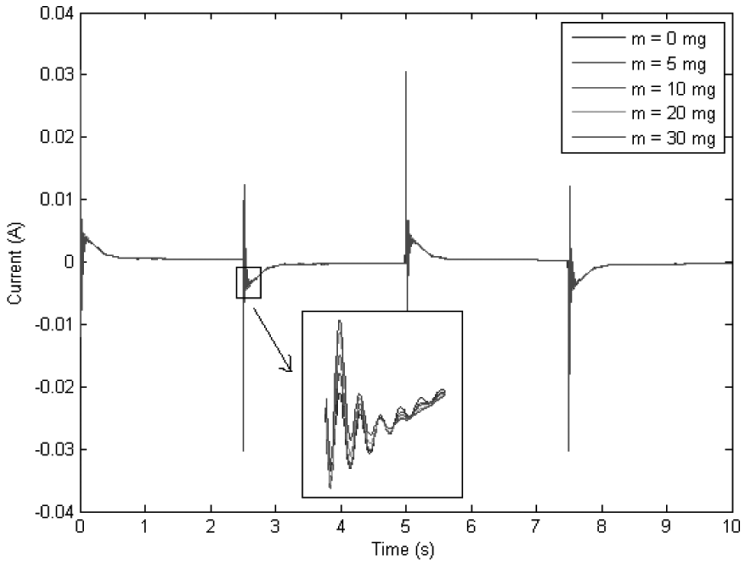


Fig. 29. Current output of the actuator for all considered uncertainty under a square wave input.

PPy actuator and variable tip loadings which allows the application of the actuator in functional devices. Simulation of design indicates that the actuator has a good and consistent performance in both tracking and disturbance rejection problems.

Future work covers

(i) investigating the effects of both geometric and material nonlinearity in the mechanical dynamics modeling (ii) employment of soft computing techniques such as Fuzzy and Neural networks plus evolutionary algorithms in the modeling and control of PPy actuators. (iii) modeling, control, and fabrication of micro robots based on fast trilayer polypyrrole bending actuators. (iv) applying the modified QFT technique in analyzing the PPy actuator as a distributed parameter system (DPS).The research is fortunately ahead of schedule and will be reported soon.

## Acknowledgment

This project is partly funded by Research Council of Ferdowsi University of Mashhad. The authors would like to sincerely thank Mr. Mahmoud Amiri Moghadam from MURSCO. for his useful comments during this work. This project is a part of a research program for achieving a new generation of actuators which can be used in micro and nano robots.

## References

[1] J.M. Hollerbach, I.W. Hunter and J. Ballantyne, A comparative analysis of actuator technologies for robotics. MIT press, 1999.

[2] W. Ian, Hunter and Serge Lafontaine, A comparison of muscle with artificial actuators, Solid-State Sensor and Actuator Workshop, 5th Technical Digest, IEEE 1992.

[3] A. Della Santa, D. De Rossi and A. Mazzoldi, Characterization and modeling of a conducting polymer muscle-like linear actuator, *Smart Materials and Structures* **6** (1997), 23–34.

[4] E. Smela, O. Inganas and I. Lundstrom, Controlled folding of microsize structures, *Science* **268** (1995), 1735–1738.

[5] K. Kaneto, M. Kaneko, Y. Min and A.G. MacDiarmid, artificial muscle: Electromechanical actuators using polyaniline films, *Synthetic Metals* **71**(1–3) (1995), 2211–2212.
[6] D.W. Madden, Conducting polymer actuators, PhD thesis, MIT, 2000.
[7] C. Zheng, S. Shatara and T. Xiaobo, Modeling of Biomimetic Robotic Fish Propelled by An Ionic Polymer – Metal Composite Caudal Fin, IEEE/ASME TRANSACTIONS ON MECHATRONICS, June, 2010.
[8] W.H. Edwin, Jager, Elisabeth Smela, Olle Ingana, Microfabricating Conjugated Polymer Actuators, www.sciencemag.org, SCIENCE, VOL 290, 24NOVEMBER 2000.
[9] A. Amir, M. Amiri, M. Moavenian and H. Ekhteraei, Modeling and Robust Control of a Soft Robot based on Conjugated Polymer Actuators. To be published in International Journal of Modelling, Identification and Control, 2010.
[10] Y. Wu et al., Fast trilayer polypyrrole bending actuators for high speed applications, *Synthetic Metals* **156** (2006), 1017–1022.
[11] W. Stephen, John et al., Validation of Resonant Frequency Model for Polypyrrole Trilayer Actuators, *IEEE/ASME Transaction on MECHATRONICS* **13**(4) (AUGUST 2008).
[12] J.D. Madden, R.A. Cush, T.S. Kanigan and I.W. Hunter, Fast contracting polypyrrole actuators, *Synthetic Metals* **113** (2000), 185–192.
[13] P.G.A. Madden, Development and modeling of conducting polymer actuators and the fabrication of a conducting polymer based feedback loop, PhD thesis, Massachusetts Institute of Technology, 2003.
[14] T.A. Bowers, Modeling, Simulation, and Control of a Polypyrrole-Based Conducting Polymer Actuator, MSc thesis, MIT, 2004.
[15] A. Amir, M. Amiri and A. Akbarzadeh, Tootoonchi, Multi-level Fuzzy-QFT Control of Conjugated Polymer Actuators, ISR/ROBOTIK 2010, pp. 1038–1045.
[16] A. Amir, M. Amiri, M. Moavenian and K. Torabi, Takagi-Sugeno Fuzzy Modelling and Parallel Distribution Compensation Control of Conducting Polymer Actuators, *Journal of Systems and Control Engineering*, 2009.
[17] K. Torabi, M. Moavenian, A.A. Amiri and A.H. Amiri, Modelling and Control of Conjugated Polymer Actuators Using Robust Control QFT, 17th Annual International Conference on Mechanical Engineering, ISME 2009.
[18] S.S. Ge, T.H. Lee and C.J. Harris, Adaptive Neural Networks Control of Robotic Manipulators, World Scientific Publishing, 1998.
[19] G. Wallace and G. Spinks, Conducting polymers – bridging the bionic interface, *Soft Matter* **3** (2007), 665–671.
[20] F. Yang et al., A scalable model for trilayer conjugated polymer actuators and its experimental validation, *Materials Science and Engineering* **28** (2008), 421–428.
[21] B. Golubev and I.M. Horowitz, Plant Rational Transfer function Approximation from Input-Output Data, *International Journal of Control* **36**(4) (1982), 711–723.
[22] F. Yang et al., Robust Adaptive Control of Conjugated Polymer Actuators, *IEEE TRANSACTIONS ON CONTROL SYSTEMS TECHNOLOGY* **16**(4) (JULY 2008).
[23] T.F. Otero and J.M. Sansinena, Bilayer dimensions and movement inartificial muscles, *Bioelectrochemistry and Bioenergetics* **42**(2) (1997), 117–122.
[24] S. Graham, Kelly, Advanced Vibration Analysis, Taylor and Francis, 2007.
[25] Leonard, Meirovitch, Elements of Vibration Analysis, Second Edition, McGraw-Hill,1986.
[26] I.M. Horowitz, *Synthesis of Feedback Systems*, Academic Press, 1963.
[27] I.M. Horowitz and M. Sidi, Synthesis of feedback systems with large plant ignorance for prescribed time domain tolerances, *Int J Control* **16** (1972), 287–3092
[28] I.M. Horowitz and M. Sidi, Optimum synthesis of nonminimum phase feedback system with plant uncertainty, *Int J Control* **27** (1978), 361–386.
[29] I.M. Horowitz, *Quantitative Feedback Design Theory* (*QFT*), volume 1. QFT Publications, 4470 Grinnel Ave., Boulder, Colorado 80303, USA, 1992.
[30] C.H. Houpis, Quantitative Feedback Theory (QFT) For the Engineer: A Paradigm for the Design of Control Systems for Uncertain Nonlinear Plants. Wright Laboratory, 1995.
[31] O. Yaniv, Quantitative Feedback Design of linear and non-linear control systems, Kluwer Academic Publication, Norwell, Massachussets, 1998.
[32] A. Amir, M. Amiri, M.R. Gharib, M. Moavenian and K. Torabi, Modelling and control of a SCARA robot using quantitative feedback theory, *Journal of Systems and Control Engineering*, 2009.